aerospace

MDPI

*Article*

# Experimental Study on Electron Extraction Characteristics of an RF Plasma Bridge Neutralizer in an Ion-Plume Environment

**Junzhe Yang [1,2], Hongbin He [1], Longfei Ma [2,3,*], Jianwu He [2,3,*], Li Duan [2,3], Qi Kang [2,3] and Jinyue Geng [2,3]**

[1] School of Aero Engine, Shenyang Aerospace University, Shenyang 110136, China; junzheyang_bbk@163.com (J.Y.); hongbinhe_mech@163.com (H.H.)
[2] Institute of Mechanics, Chinese Academy of Sciences, Beijing 100190, China; duanli@imech.ac.cn (L.D.); kq@imech.ac.cn (Q.K.)
[3] School of Engineering Sciences, University of Chinese Academy of Sciences, Beijing 101408, China
* Correspondence: malf@imech.ac.cn (L.M.); javehe@imech.ac.cn (J.H.)

**Abstract**

Systematic experimental characterization of the electron extraction characteristics of a radio-frequency plasma bridge neutralizer (RPN) in the actual ion-plume environment of a radio-frequency ion thruster (RIT) remains limited, particularly regarding the effects of ion-beam conditions and the relative configuration between the RIT and RPN. In this study, an experiment consisting of an RIT-13 and an RPN-2.5 was established, in which the RIT-13 operated with an Xe + $N_2$ + $O_2$ mixed propellant and the RPN-2.5 operated with Xe. Experimental investigations were conducted to systematically examine the effects of collector bias voltage, ion beam current, screen-grid voltage, RPN installation angle, and spatial position on electron extraction. The results show that the collector bias voltage is the primary parameter governing the electron extraction state, and two distinct jumps occur as the magnitude of the negative collector bias voltage increases, while the ion beam current mainly modulates the electron extraction state near the threshold of the first jump. The 60° and 90° configurations generally exhibit stronger electron extraction capability than the 0° and 30° configurations and require smaller magnitudes of negative collector bias voltage to reach the high-current electron extraction state. A pronounced spatial dependence is also observed. At an ion beam current of approximately 440 mA and a screen-grid voltage of 1200 V, the region of X = −10 mm and Y = 20–40 mm exhibits favorable electron extraction characteristics. Among the investigated configurations, the 90° configuration at (−10, 40) mm requires the smallest magnitude of collector bias voltage, approximately 13.5–14 V, for the RPN electron extraction current to match the RIT ion beam current. This current-matching bias is defined in the present study as the equivalent floating potential $U_{eq}$. These results provide an experimental basis for the matching design and spatial configuration of RITs and RPNs in an air-breathing electric propulsion system.

**Keywords:** air-breathing electric propulsion system; radio-frequency ion thruster; radio-frequency plasma bridge neutralizer; electron extraction characteristics; ion plume

Check for updates

Academic Editor: Patrick J. Norman

Received: 28 August 2026
Revised: 15 September 2026
Accepted: 18 September 2026
Published: 21 September 2026

**Copyright:** © 2026 by the authors. Licensee MDPI, Basel, Switzerland. This article is an open access article distributed under the terms and conditions of the Creative Commons Attribution (CC BY) license.

## 1. Introduction

Very low Earth orbit (VLEO) is generally defined as the orbital altitude range of 100–350 km and corresponds to the low-altitude region near the upper boundary of the dense atmosphere. In recent years, with advances in high-resolution Earth observation, low-latency communications, and small-spacecraft technologies, VLEO has attracted increasing attention for near-Earth space missions [1]. Compared with conventional low Earth orbit

(LEO), lower orbital altitude can improve the spatial resolution of remote-sensing payloads and, for a given imaging performance, potentially reduce the required payload size and power consumption [2]. The reduced satellite-to-ground propagation distance also provides favorable conditions for low-latency communications. In addition, the low altitude may offer opportunities for reducing launch and mission costs. However, the atmospheric density in VLEO is substantially higher than that in conventional LEO, resulting in increased aerodynamic drag and continuous losses of orbital energy and altitude. Therefore, a continuous low-power propulsion system for aerodynamic-drag compensation is one of the key technologies for the long-term operation of VLEO spacecraft [3].

The rarefied atmosphere in VLEO consists predominantly of atomic oxygen and molecular nitrogen, providing the possibility of utilizing in situ atmospheric resources as propellant. Air-breathing electric propulsion (ABEP) captures the atmospheric gas encountered by a spacecraft during flight and uses it as propellant, which is subsequently ionized, extracted, and accelerated to generate thrust for aerodynamic-drag compensation [4]. Compared with conventional electric propulsion systems relying on stored propellant, ABEP can reduce the dependence of long-term VLEO operation on onboard propellant reserves and is therefore considered a promising approach for sustained aerodynamic-drag compensation and extended mission lifetime [5]. A comprehensive review by Andreussi et al. [6] summarized the development of ABEP from mission studies to technology verification, including air-intake concepts, electric thrusters, neutralization technologies, and ground-based verification strategies. The RIT concept was introduced by Löb in the early 1960s [7]. In an RIT, plasma is generated in the discharge chamber by radio-frequency inductive coupling, and positive ions are extracted and accelerated through an ion optics system to generate thrust [8]. RITs offer high specific impulse, adjustable thrust, long lifetime, and broad propellant compatibility, making them well suited to ABEP. However, an RIT requires a neutralizer to provide an electron current sufficient to compensate for the extracted ion beam current and maintain spacecraft charge balance. Insufficient electron emission can lead to spacecraft charging [9] and modify the potential distribution and charged-particle transport in the plume [10]. These effects may increase the risk of ion backflow and particle bombardment of spacecraft surfaces, thereby compromising the long-term operation of sensitive spacecraft components and the propulsion system. The relatively high atomic oxygen content of the VLEO environment imposes stringent requirements on the environmental compatibility and long-term reliability of electric propulsion system. Conventional hollow cathodes commonly employ thermionic emitters such as impregnated barium–tungsten (Ba–W) and lanthanum hexaboride ($LaB_6$). Ba–W emitters are particularly susceptible to oxygen and other reactive impurities and generally require high-purity inert-gas propellants; exposure to oxygen-rich environments can degrade their electron emission performance [11,12]. In contrast, an RPN does not rely on a conventional thermionic emitter. Instead, plasma is generated directly through inductively coupled plasma discharge, from which electrons are extracted. This configuration avoids some of the lifetime limitations associated with emitter poisoning and depletion and therefore provides potential advantages for operation in oxygen-containing environments. However, the RPN in the present experiments was operated with Xe, and its oxygen tolerance was not directly evaluated in this study.

Early studies explored different insert-free RPN concepts. Weis et al. investigated electron extraction from a capacitively coupled RF discharge, while Godyak et al. developed an inductively coupled RPN and characterized the effects of RF power, gas pressure, and extraction voltage on electron emission [13,14]. Raitses et al. subsequently performed a parametric investigation of electron extraction from a low-frequency inductively coupled RF plasma source, considering extraction voltage, electrode spacing, RF power, and xenon

flow rate [15]. In 2007 and 2009, Hatakeyama et al. [16] first reported the development of the RF neutralizer, and Watanabe et al. [17] subsequently further characterized the device, reporting an electron extraction current of 2.1 A at an RF power of 100 W, a xenon flow rate of 2 sccm, and a target voltage of 40 V. Since 2005, Longmier and Hershkowitz [18] have conducted systematic investigations of RF plasma cathodes, focusing on the relationships among extracted electron current, plasma density, propellant flow rate, and ion-collector area. Their theoretical analysis showed that, when electrons and ions are lost to the grounded ring and ion collector, respectively, current balance can be established when the ratio of the two collection areas approximately equals the square root of the electron-to-ion mass ratio. Under this condition, the extractable electron current approaches the random electron flux. An extracted electron current of 3.75 A was obtained at an RF power of 340 W. In 2007, they [19] compared xenon and argon as propellants and demonstrated the performance advantages of xenon. An electron extraction current of 30 A was achieved at 13.56 MHz, an RF power of 1300 W, and a xenon flow rate of 2 sccm. A transition to the helicon mode was also observed at an RF power of 1000 W, an argon flow rate of 15 sccm, and an externally applied magnetic field of 100 G. In 2009, Longmier et al. [20] further investigated nonequilibrium anodic double layers associated with positively biased planar electrodes immersed in plasma. Under global nonambipolar flow conditions, the difference between electron and ion transport rates leads to the formation of an ion-rich region adjacent to the electron sheath near the positively biased electrode, resulting in an anodic double layer. As the electrode bias voltage increases, the near-electrode plasma structure evolves successively through electron-sheath, anode-glow, and anode-spot regimes. The critical bias voltage for the transition to the anode-spot regime was found to be inversely proportional to the neutral gas pressure, while the electron current collected by the electrode exhibits pronounced hysteresis. In 2016, Jahanbakhsh et al. [21] experimentally investigated electron extraction from an RF plasma cathode and systematically examined the effects of discharge-chamber diameter and length, emission-aperture geometry, RF power, and propellant flow rate. The results demonstrated that the electron extraction characteristics of RF plasma cathodes depend strongly on both geometric configuration and operating parameters. In 2018, Jianwu He et al. [22] developed a compact inductively coupled RPN-1. Rapid ignition was achieved by applying a pulsed high voltage to an internal probe to generate seed electrons. They also introduced the anode-plate concept into the analysis of RPN and proposed that variations in the ratio of the emission-aperture area to the internal collector area modify the sheath structure near the emission aperture, thereby affecting the electron extraction. In 2019, Xingda Li et al. [23] conducted numerical simulations and experiments on a 1-A-class RF neutralizer. Good agreement was obtained between the numerical and experimental results, and an optimum condition for electron extraction was identified. Under the rated operating condition, the prototype exhibited a discharge loss of 99 W/A, a propellant utilization factor of 11, and a maximum saturated electron current of 2 A. In 2022, Zongqi Xu et al. [24] developed an RF plasma cathode employing a graphite ion collector. Their results showed that the electron extraction current gradually approached saturation with increasing RF power or propellant flow rate. In 2024, Jiahao Fu et al. [25] developed a long-lifetime, oxidation-resistant, 1-A-class xenon-fed RPN and systematically investigated the influence of the emission-aperture diameter on electron extraction. The discharge chamber had an inner diameter and length of 40 mm, and a C-shaped molybdenum collector fabricated from a 100 mm × 40 mm × 0.3 mm sheet was installed inside the discharge chamber. Emission-aperture diameters of 1–4 mm were investigated at an RF frequency of 1.6 MHz. In particular, for a 2 mm emission aperture and an RF input power of 55 W, two distinct jumps in electron extraction current were observed at Xe flow rates of 0.5 and 0.6 sccm, whereas only one jump was observed at 0.4 sccm.

Considering the propellant utilization factor and electron extraction power consumption, an emission-aperture diameter of 1.5 mm was identified as the preferred configuration; at an electron extraction current of 1 A and an RF power of 55 W, the corresponding Xe flow rate was 0.5–0.6 sccm. More recently, Zorn et al. [26] characterized an RIT-10 and an RPN as candidate subsystems for ABEP using molecular $O_2$ and $N_2$. The RIT-10 was additionally investigated with $O_2/N_2$ mixtures, whereas the RPN was characterized separately with $O_2$ and $N_2$. Electron extraction from the RPN was achieved using an external biased graphite anode, and the effects of excitation frequency and propellant flow rate on the extracted current and plasma parameters were investigated. Their results highlighted the importance of reactive-gas chemistry, operating parameters, and material compatibility for RF-based propulsion and neutralization devices intended for ABEP applications.

Coupled operation between RPN and RITs has also been demonstrated. Neumann et al. reported the first coupled test of a cathodeless RPN with an RIT-22 ion thruster [27], based on the RPN developed by Scholze et al. [28]. These studies demonstrated the feasibility of RPN operation in conjunction with an actual ion thruster. Related studies of Hall-effect thruster–hollow-cathode systems have also established that cathode position can significantly affect cathode coupling voltage and the near-field plasma environment [29,30]. Although the thruster and electron-source configurations differ from the RIT–RPN system considered here, these studies establish the broader importance of electron-source position in thruster–neutralizer coupling. The spatial coupling between an electron source and an ion plume is also known to depend on the neutralizer position. Using fully kinetic simulations of a gridded ion-thruster plume, Nishii and Levin [10] showed that the neutralizer position significantly affects electron transport, plume potential, and the degree of ion-beam neutralization. They also demonstrated substantial differences between in-chamber and in-space plume neutralization owing to the electrical boundary conditions imposed by grounded vacuum-chamber walls. These results demonstrate the importance of neutralizer position and facility effects for ion-beam neutralization; however, the study considered plume-scale electron transport numerically rather than the experimentally measured electron extraction characteristics of an RPN.

Although these studies have established the fundamental electron-extraction characteristics of RPNs, many experimental investigations employ an anode plate to simulate the ion plume of a thruster, with the current collected by the anode plate used to characterize the electron-emission capability of the neutralizer. However, in an actual electric propulsion system, the neutralizer does not operate independently. Its electron extraction process is coupled to the ion beam current produced by the thruster and is therefore influenced by parameters such as beam current, ion energy, and the relative spatial position between the neutralizer and the ion beam. During thruster operation, the ion plume not only provides the charge-compensation environment for electrons emitted by the neutralizer but also modifies the local plasma potential and electrical-field distribution around the neutralizer emission aperture. Moreover, the thruster and neutralizer form a coupled electrical system in which their operating potential are not independently prescribed. Consequently, the electron emission state of the neutralizer must adjust to changes in the ion beam and plasma environment to maintain the overall current and potential balance of the propulsion system. In this study, an RIT-13 RF ion thruster and an RPN-2.5 RF plasma bridge neutralizer were employed. A variable collector bias voltage was applied to the neutralizer collector to characterize the electron extraction behavior of the RPN in the actual ion plume generated by the RIT. The experiments systematically investigated the effects of collector bias voltage, ion beam current, screen-grid voltage, neutralizer installation angle relative to the ion beam (0°, 30°, 60°, and 90°), and neutralizer spatial position. In addition, bidirectional sweeps of the collector bias voltage were performed to examine the possible hysteresis

behavior of the electron extraction process. The results provide experimental insight into the coupling between the RIT ion plume and RPN electron extraction and provide a basis for optimizing the operating conditions and spatial configuration of RPNs in air-breathing electric propulsion system.

## 2. Operating Principle and Experimental Setup

### *2.1. Operating Principle*

The experimental system mainly consists of an RIT, an RPN, an RF power supply, a high-voltage power supply, and a propellant storage and supply unit, as shown in Figure 1. For the RIT, the ion beam current and ion energy were varied by adjusting the RF power and screen-grid voltage, respectively, thereby enabling systematic investigation of their effects on the electron extraction characteristics of the RPN. The electron extraction current of the RPN is governed not only by its RF power and propellant flow rate but also by the potential distribution between the plasma inside the RPN discharge chamber and the surrounding plasma environment. As shown in Figure 1, the collector bias voltage (CBV3) applies an adjustable negative voltage to the RPN collector, thereby modifying the potential distribution between the RPN plasma and the external environment and consequently controlling the electron extraction conditions.

$$U_e = U_S - U_{coll} \tag{1}$$

where $U_e$ is the electron extraction voltage, $U_S$ is the potential of the RIT ion plume, and $U_{coll}$ is the negative collector bias voltage applied to the RPN collector. The corresponding electron extraction current $I_e$ can then be measured and used to characterize the electron extraction characteristics of the RPN. The local plume potential $U_S$ was not measured directly in the present study; therefore, $U_e$ was not quantitatively evaluated, and the experimental results are presented as functions of the directly controlled collector bias voltage $U_{coll}$.

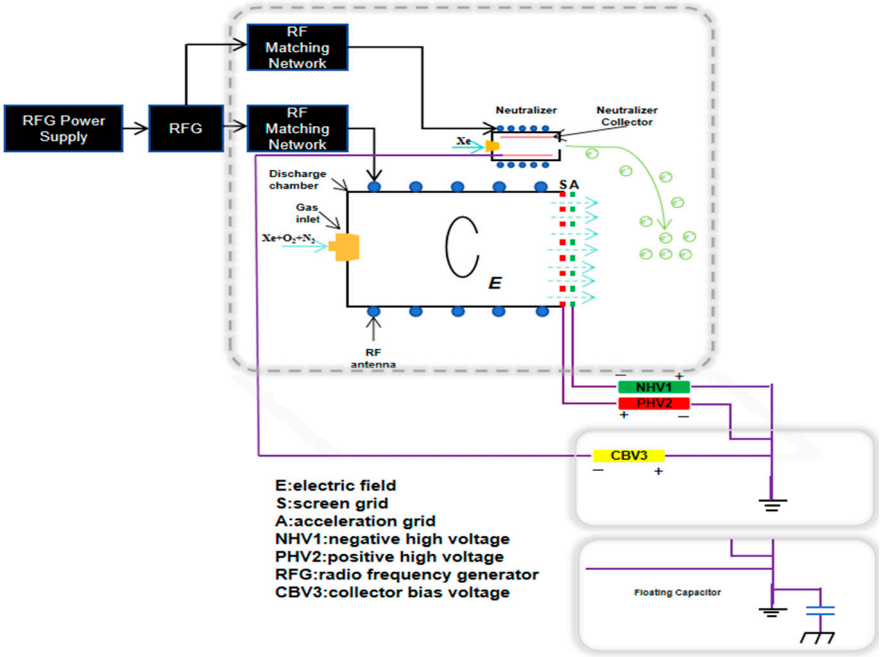



**Figure 1.** Schematic diagram of the operating principle of the RF ion propulsion system.

When the RIT and RPN operate in orbit, the thruster grids and the RPN collector form an electrically floating system, as illustrated in the lower-right part of Figure 1. The

potential of the RPN collector varies with the floating potential of the system, thereby regulating the potential difference between the plasma inside the RPN and the surrounding ion plume. This potential difference determines the electron extraction conditions and, consequently, the electron emission capability of the RPN. As the system approaches a steady state, the net current gradually decreases until a stable current-balance condition is established.

$$I_b = I_s - I_a \tag{2}$$

where $I_b$ is the ion emission current of the RIT, $I_s$ is the current measured by the positive high-voltage power supply connected to the screen-grid, and $I_a$ is the magnitude of the ion current intercepted by the accelerator-grid and measured by the negative high-voltage power supply. Both power supplies are capable of measuring the several-hundred-milliampere current levels encountered in the present experiments, with a current-reading resolution of 0.1 mA, and were verified prior to the experiments.

$$C\frac{dU_f}{dt} = I_e - I_b + I_{other} \tag{3}$$

where $C$ represents the effective capacitance of the electrically floating spacecraft–propulsion system with respect to the surrounding ambient plasma, $U_f$ is the floating potential, and $I_e$ is the electron extraction current of the RPN. Here, $C$ is a lumped parameter describing the charging response of the floating system rather than a physical capacitor inserted into the propulsion circuit. Since secondary-electron currents and other minor current components are relatively small, they can be neglected.

$$I_{other} \approx 0 \tag{4}$$

Therefore, when the RIT and RPN operate under steady-state conditions,

$$\frac{dU_f}{dt} = 0 \tag{5}$$

$$I_e = I_b \tag{6}$$

Based on the current-balance relationship described above, the collector bias voltage $U_{coll}$ is actively adjusted using CBV3 to modify the potential relationship difference between the plasma inside the RPN and the surrounding ion plume, while the corresponding electron extraction current $I_e$ is measured simultaneously. For a given RIT ion beam current $I_b$ and RPN spatial position, the dependence of the electron extraction current on the collector bias potential can be obtained by continuously varying $U_{coll}$. When the collector bias potential reaches a specific value $U_{eq}$, the electron extraction current of the RPN satisfies

$$I_e(U_{eq}) = I_b \tag{7}$$

In the present ground experiment, the collector bias corresponding to the current-matching condition is operationally defined as

$$U_{eq} = U_{coll}|_{I_b = I_e} \tag{8}$$

Here, the term "equivalent" refers to the equivalence of the current-balance operating condition rather than to equality of absolute electrostatic potentials. Therefore, $U_{eq}$ should not be interpreted as a direct measurement of, or as being numerically identical to, the actual on-orbit floating potential $U_f$. During on-orbit operation, the floating potential adjusts self-consistently according to the charging balance of the electrically floating

spacecraft–propulsion system and the surrounding plasma environment, and its absolute value depends on the corresponding plasma and electrical boundary conditions. In the present study, $U_{eq}$ is therefore used as a current-balance-derived comparative parameter for evaluating the relative matching characteristics of different RIT–RPN configurations under the investigated ground-test conditions.

### *2.2. Experimental Scheme*

The experimental platform was established using a ground-based space-vacuum simulation system, as shown in Figure 2. The vacuum chamber can reach a base pressure on the order of $10^{-4}$ Pa. After the RIT and RPN reach stable operation, the chamber pressure remains below $3 \times 10^{-3}$ Pa, satisfying the operating requirements of both devices. The experimental parameters of the RIT-13 and RPN-2.5 are listed in Table 1.



**Figure 2.** Ground-based experimental platform for space-vacuum environment simulation.

**Table 1.** Experimental parameters.

| | Propellant | Effective RF Power | Screen-Grid Voltage | Accelerator-Grid Voltage | Collector Bias Voltage |
|---|---|---|---|---|---|
| RIT-13 | Xe + $N_2$ + $O_2$ (2 sccm + 10 sccm + 10 sccm) | 80 W~280 W | 1000 V/1200 V | −150 V | - |
| RPN-2.5 | Xe (0.8 sccm) | 20 W | - | - | −5~−25 V |

The Xe–$N_2$–$O_2$ mixture used for the RIT was not intended to reproduce the atmospheric composition at a specific VLEO altitude. $N_2$ and $O_2$ constitute the major fraction of the supplied gas, while a small Xe admixture, corresponding to approximately 10% of the total RIT flow rate, was retained to support ignition and ionization of the mixed-gas discharge.

In this study, the effective RF power is defined as the difference between the forward RF power and the reflected RF power. The RPN employs a quartz discharge chamber and a tantalum collector. The collector has an outer diameter of 25 mm, a thickness of 0.8 mm, a length of 55 mm, and an opening angle of 10°. The diameter of the RPN electron-emission aperture is 1.5 mm, and the RF operating frequency is 4 MHz. The RIT likewise employs a quartz discharge chamber. Its screen-grid is made of molybdenum, whereas the accelerator-grid is made of graphite. The thruster diameter is 13 cm, and the RF operating frequency is 1 MHz.

To evaluate whether the collector current could be affected by direct ion collection from the RIT plume, a control test was performed with the RPN RF power switched off while the RIT remained in operation. The collector bias voltage was swept from −5 to −25 V, and no resolvable collector current was indicated within the 0.1 mA current-reading resolution of the CBV3 power supply. The collector is located inside the RPN discharge chamber, while the surrounding external structure is electrically insulating. This control result indicates that direct collection of plume ions by the RPN collector did not produce a measurable contribution to the collector current under the investigated configuration.

To further investigate the spatial coupling characteristics between the ion plume and the RPN, the installation angle of the RPN relative to the RIT was varied among 0°, 30°, 60°, and 90°, as shown in Figure 3. Considering the practical integration of the RIT and RPN, the installation angle investigated in this study was not varied by rotating the RPN about the center of its emission aperture. As illustrated in Figure 3, the RPN was rotated about an axis located at the edge of the RIT. Consequently, changing the installation angle modifies not only the orientation of the RPN relative to the ion-beam direction but also the geometrical position of the emission aperture relative to the RIT and its ion plume. This arrangement was adopted to represent the relative RIT–RPN geometry associated with practical engineering integration more closely. A three-degree-of-freedom positioning stage was used to adjust the spatial position and installation angle of the RPN. The positioning stage provides translational motion along the X and Y axes, and rotational motion about an axis perpendicular to the XY plane, thereby enabling precise adjustment of the RPN position and installation angle for different experimental configurations. Figure 4 shows photographs of the RPN installed angles at 0° and 30° relative to the RIT after adjustment using the positioning stage.

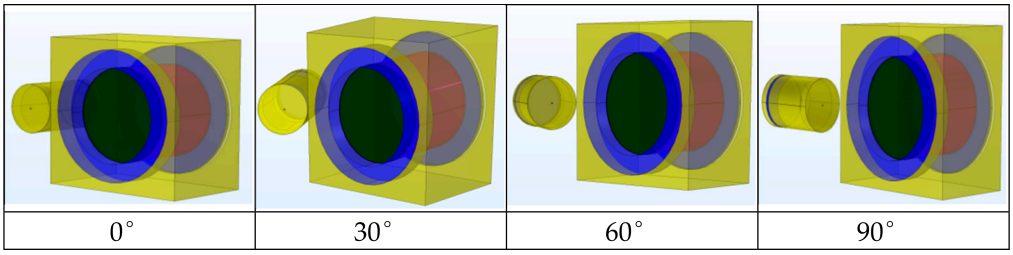



**Figure 3.** Schematic of the installation angles between the RPN and RIT.

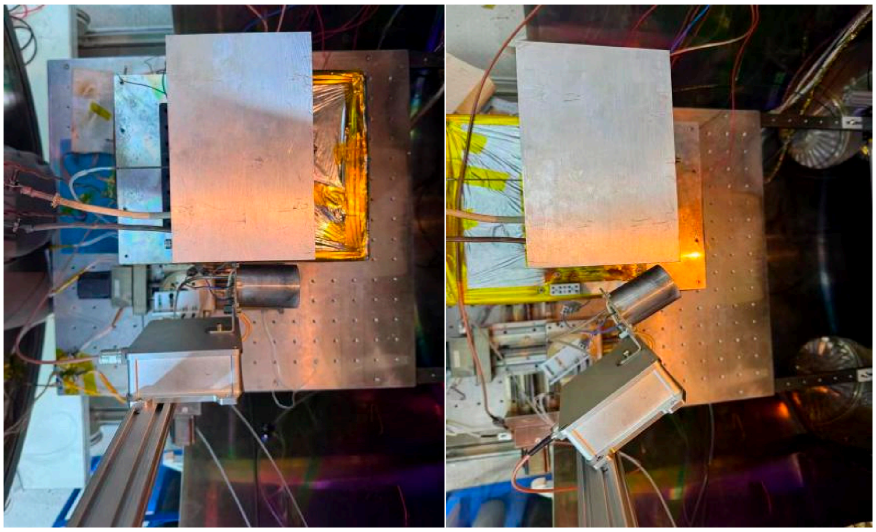


**Figure 4.** The RPN and RIT at installation angles of 0° and 30°.

During the collector-bias-voltage sweep, the collector bias was adjusted from −5 to −25 V and then returned from −25 to −5 V in increments of 0.1 V. The measurements were performed quasi-statically. After each voltage adjustment, the discharge state and current reading were checked for stabilization before proceeding to the next voltage point. Therefore, no fixed continuous scan rate or prescribed dwell time was used. For clarity of presentation, selected data points at 2 V intervals are shown in the figures, whereas the actual voltage-adjustment step during the experiments was 0.1 V. Each operating condition was measured twice, and the typical run-to-run difference in the electron extraction current was approximately 5 mA.

## 3. Experimental Results and Analysis

### *3.1. Effects of Ion Beam Current and Collector Bias Voltage on Electron Extraction*

Fu et al. [25] investigated the electron extraction characteristics of an RPN and reported distinct jumps as the anode-plate bias voltage was increased. Once the anode spot and plasma bridge were established, the neutralizer could maintain a high-current electron extraction state over a certain range of bias voltage, accompanied by a pronounced hysteresis effect. In this section, the RIT screen-grid voltage was set to 1200 V and the accelerator-grid voltage to −150 V. Under these conditions, the effects of ion beam current and collector bias voltage on the electron extraction characteristics of the RPN were systematically investigated.

As shown in Figure 5, "+" denotes an increasing sweep of the magnitude of the collector bias voltage, whereas "−" denotes a decreasing sweep. With the RIT ion beam current maintained at approximately 430 mA and the RPN installation angle varied from 0° to 90°, two distinct jumps were observed. The electron extraction current therefore did not increase continuously with the magnitude of the applied collector bias voltage but instead exhibited abrupt increases within specific collector bias-voltage ranges, consistent with the behavior reported in Ref. [25]. When the collector bias voltage reached a critical value, the abrupt increase in electron extraction current, together with the pronounced luminous emission observed near the RPN emission aperture, was qualitatively consistent with the formation of an anode-spot-like state reported in Ref. [25]. The first current jump may therefore be associated with an increase in the local plasma density near the emission aperture accompanying such a discharge-state transition, which could enhance electron extraction. With a further increase in the magnitude of the negative collector bias voltage, the second current jump may be associated with enhanced plasma production and transport in the region between the emission aperture and the surrounding plasma environment. This process may promote the establishment of a more strongly coupled plasma-bridge-like state and thereby contribute to the transition toward the high-current electron extraction state. Because no spatially resolved plasma diagnostics were performed in the present study, these interpretations remain qualitative and should be regarded as literature-supported physical explanations rather than directly demonstrated mechanisms. Taking the 0° configuration as an example, when the collector bias voltage reached −11 V, the first pronounced jump occurred, with the electron extraction current increasing from approximately 50 mA to 175 mA. As the magnitude of the negative collector bias voltage was further increased, the electron extraction current continued to rise. When the collector bias voltage reached −21 V, a second pronounced jump occurred, and the electron extraction current increased from approximately 350 mA to 625 mA, after which the current approached a saturated extraction state. These results indicate that multistage current-jump behavior can also occur in the ion-plume environment of the RIT as the collector bias voltage of the RPN is varied. However, no pronounced hysteresis was observed between the increasing and decreasing collector

bias-voltage sweeps, indicating that the electron extraction state remained largely reversible with respect to changes in collector bias voltage over the investigated operating range.

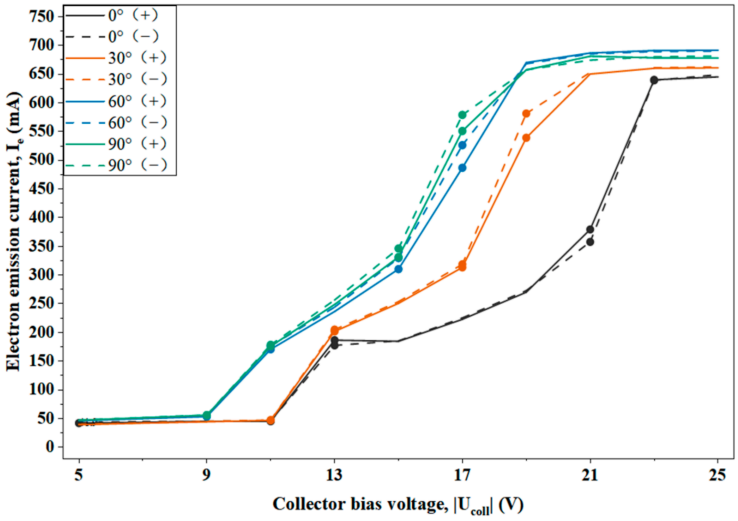



**Figure 5.** Effect of collector bias voltage on the electron extraction current.

Unlike the experimental conditions in Ref. [25], in which a fixed anode plate was used as the electron collection boundary, the RPN in this study operates directly within the ion plume generated by the RIT. This difference in the external boundary condition may contribute to the reduced hysteresis observed in these experiments. The ion plume provides a continuous flux of charged particles and establishes a dynamic electrical coupling with the electron current emitted by the RPN. Changes in electron and ion transport modify the local plasma potential and sheath structure around the RPN emission aperture, which in turn affects the electron extraction process. Such self-consistent electrostatic coupling may provide a stabilizing feedback mechanism that suppresses the persistence of different plasma states during forward and reverse bias sweeps, thereby weakening the hysteresis behavior.

Figure 6 presents the electron extraction characteristics of the RPN at installation angles of 0°, 30°, 60°, and 90° under different RIT ion beam currents and collector bias voltages. The experimental results show that the RIT ion beam current has a relatively limited influence on the electron extraction current. In particular, after the RPN enters the high-current electron extraction state, the electron extraction current becomes less sensitive to variations in ion beam current. However, when the collector bias voltage is close to the threshold for the first jump, changes in ion beam current still modulate the electron extraction state, promoting the transition from the low-current state to the higher-current state following the first jump. Taking the 30° configuration as an example, at a collector bias voltage of −13 V, the electron extraction current undergoes the first jump when the ion beam current increases to approximately 350 mA. In contrast, when the magnitude of the collector bias voltage is reduced to −9 V, no first jump is observed within the investigated ion beam current range. When the magnitude of the collector bias voltage is increased to −17 V, the RPN has already transitioned to the electron extraction state following the first jump. These results indicate that the ion beam current can influence the electron extraction state within the current-jump transition region, but its effect depends strongly on the collector bias voltage.

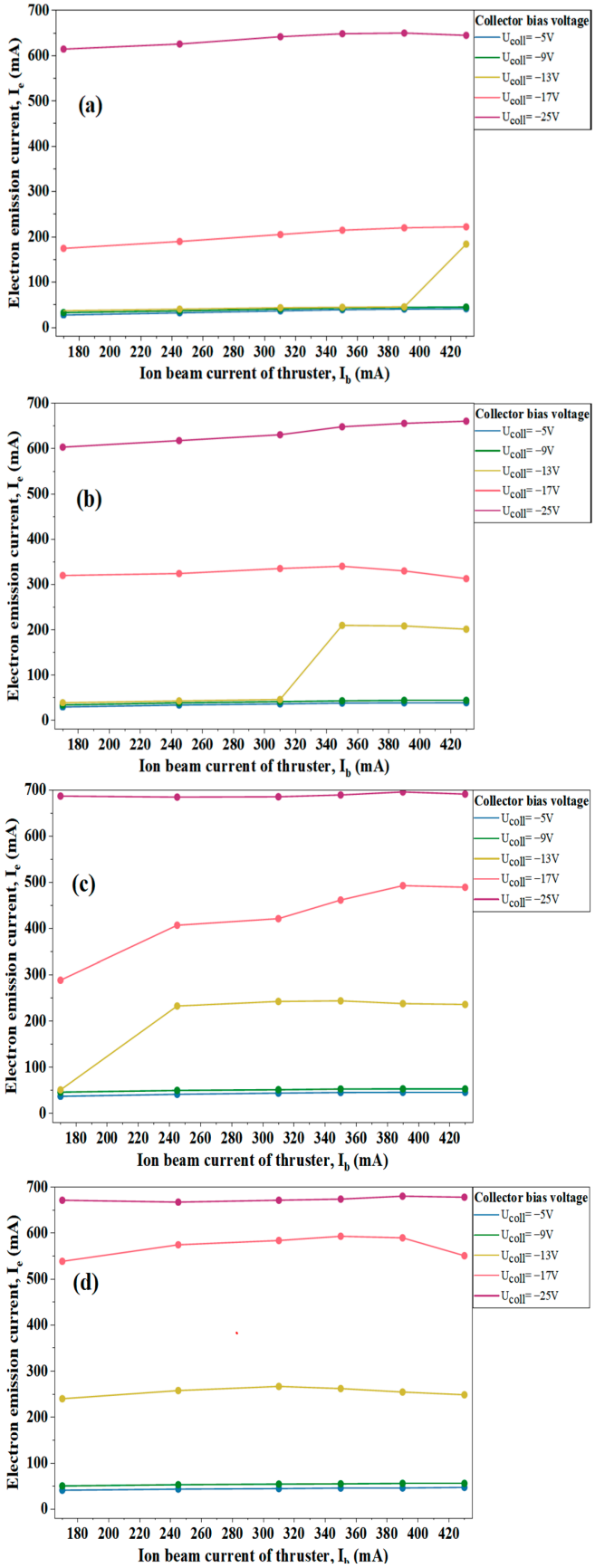



**Figure 6.** Effects of ion beam current and installation angle on the electron extraction current. (**a**) RPN installation angle relative to the RIT: 0°; (**b**) RPN installation angle relative to the RIT: 30°; (**c**) RPN installation angle relative to the RIT: 60°; (**d**) RPN installation angle relative to the RIT: 90°.

The electron extraction characteristics also vary significantly with the RPN installation angle, particularly in terms of the collector bias voltage required to trigger the jumps and the corresponding electron extraction current. At a collector bias voltage of −13 V, the electron extraction current under the 0° configuration generally remains at a relatively low level, although local transitions occur under certain ion beam current conditions. As the installation angle increases to 30°, the first jump occurs within the investigated ion beam current range. Under the 60° and 90° configurations, the first jump has already largely occurred at a collector bias voltage of −13 V, indicating that the magnitude of the collector bias voltage required to initiate the first jump decreases with increasing installation angle. When the magnitude of the collector bias voltage is further increased to −17 V, the electron extraction state progressively shifts from the post-first-jump regime toward the second jump regime as the installation angle increases.

### *3.2. Effect of RIT Screen-Grid Voltage on RPN Electron Extraction*

Two ion beam current conditions, approximately 310 mA and 440 mA, were selected for comparison. For each ion beam current, the RIT screen-grid voltage was set to 1000 V and 1200 V, and the effective RIT RF power was adjusted to match the net ion beam current between the two screen-grid-voltage conditions. In this procedure, the RF power served as a matching parameter to compensate for changes in the extracted ion flux. Because variation in the RF power also modifies the plasma-generation state in the RIT discharge chamber, the two cases should not be interpreted as differing only in screen-grid voltage. Rather, the comparison represents different RIT ion-optics operating conditions at an approximately matched net ion beam current. The RPN collector bias voltage was then varied to examine the corresponding electron extraction characteristics.

Figure 7 presents the electron extraction characteristics of the RPN at different installation angles under ion beam currents of approximately 310 mA and 440 mA for screen-grid voltages of 1000 V and 1200 V. Overall, varying the screen-grid voltage has little effect on the saturated electron extraction current at high collector-bias magnitudes but primarily shifts the collector-bias range associated with the transition from the low-current to the high-current extraction state. The magnitude of this effect also depends on the ion beam current. At an ion beam current of approximately 310 mA, the electron extraction current at a screen-grid voltage of 1200 V is generally higher than that at 1000 V within the current-jump transition region. When the ion beam current increases to approximately 440 mA, a different trend is observed under the 60° configuration. At a collector bias voltage of −17 V, the electron extraction current is approximately 550 mA at a screen-grid voltage of 1000 V, compared with approximately 430 mA at 1200 V. This indicates that, at the higher ion beam current, the RPN can reach the high-current electron extraction state at a smaller magnitude of collector bias voltage when the screen-grid voltage is 1000 V. As the magnitude of the collector bias is further increased and the electron extraction current approaches the high-current plateau, the difference between the two screen-grid voltage conditions decreases substantially. These results indicate that the primary effect of the screen-grid voltage is to modify the collector-bias condition required to trigger the current-jump transition rather than to substantially change the maximum electron extraction current attainable by the RPN.

The observed differences may be associated with the combined effects of screen-grid voltage and ion beam current on the operating state of the RIT ion optics system. Variations in screen-grid voltage not only change the ion acceleration energy but may also modify the ion extraction conditions of the grid system as well as the focusing and divergence characteristics of the ion beam. Meanwhile, variations in ion beam current alter the space-charge conditions within the grid system. Therefore, even at the same total ion beam

current, the local ion current density, ion density, plume potential, and spatial distribution near the RPN emission aperture may differ under different screen-grid voltages. As the ion beam current further increases, the operating state of the ion optics system changes accordingly, which may alter the relative local ion-plume conditions established at 1000 V and 1200 V. Consequently, the effect of screen-grid voltage on electron extraction does not necessarily exhibit a simple monotonic dependence and may even show opposite trends at different ion beam currents.

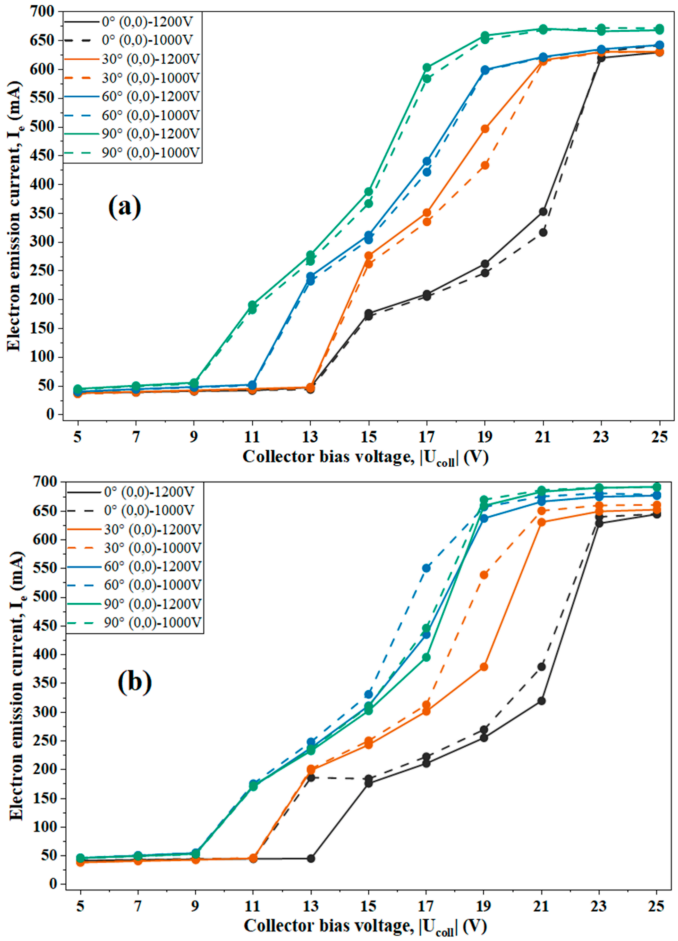



**Figure 7.** Variation in electron extraction current with collector bias voltage under different ion beam current conditions at the baseline spatial position (0, 0). (**a**) RIT ion beam current: 310 mA; (**b**) RIT ion beam current: 440 mA.

### *3.3. Effect of RPN Spatial Position on Electron Extraction*

To further examine whether the electron extraction characteristics described above remain consistent at different spatial positions, two additional RPN positions were selected for comparative experiments in addition to the different installation angles. The positive Y-axis was defined along the axial direction of the RIT ion beam, and Y = 0 corresponding to the reference position where the RIT exit plane and the plane of the RPN emission aperture were aligned. The RPN was translated along the Y-axis in 10 mm increments to vary its axial position relative to the RIT exit plane. The positive X-axis was defined perpendicular to the ion beam axis and directed radially outward from the RIT, with X = 0 corresponding to the reference transverse position. The RPN was similarly translated along the X-axis in 10 mm increments to vary its transverse distance relative to the ion beam centerline. This two-dimensional coordinate system enabled systematic comparison of the electron extraction characteristics at different axial and transverse positions and facilitated

evaluation of the effects of ion beam current, screen-grid voltage, and collector bias voltage as a function of RPN position. The investigated RPN positions are shown in Figure 8.

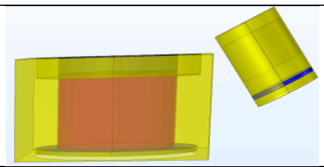
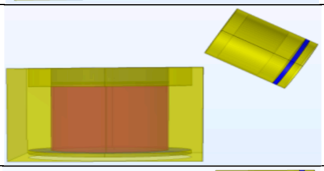
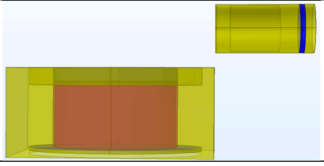
| | |
|---|---|
| 30° |  |
| 60° |  |
| 90° |  |
| | (0, 20) |

**Figure 8.** Schematic of the (0, 20) position at different installation angles.

Figure 9 presents the effects of installation angle, screen-grid voltage, and ion beam current on the electron extraction characteristics of the RPN at the spatial position (0, 20). A comparison of Figures 6 and 9 shows that the overall trends in electron extraction characteristics are highly consistent between the (0, 0) and (0, 20) positions. This consistency indicates that the observed effects of collector bias voltage, screen-grid voltage, and RPN installation angle on electron extraction are not restricted to a single spatial position.

As shown in Figures 7 and 9, at different spatial positions, the electron extraction current exhibits pronounced nonlinear growth as the magnitude of the negative collector bias voltage increases, with two distinct jumps occurring successively. Following the first jump, the RPN transitions from a low-current electron extraction state to a higher-current state. As the magnitude of the negative collector bias voltage is further increased, a second jump occurs, after which the electron extraction current gradually approaches saturation. The collector bias conditions associated with the jumps also vary significantly with the RPN installation angle. In general, under the 60° and 90° configurations, the first jump occurs at a smaller magnitude of negative collector bias voltage, and the RPN reaches the high-current electron extraction state following the second jump at a lower bias-voltage magnitude than under the 0° and 30° configurations. By contrast, the 0° and 30° configurations generally require a larger magnitude of negative collector bias voltage to achieve comparable electron extraction current. Therefore, at the same ion beam current and collector bias voltage, the 60° and 90° configurations generally exhibit higher electron extraction currents and require smaller bias-voltage magnitudes to trigger the current-jump transitions. From the perspective of potential distribution, changing the RPN installation angle alters the position and orientation of the emission aperture relative to the spatial potential distribution within the ion plume. Because the plume potential is spatially nonuniform, the local plasma potential near the emission aperture may differ with installation angles. A larger effective potential difference between the local plume potential and the RPN collector potential can reduce the potential barrier for electrons traveling from the RPN plasma through the emission-aperture region into the surrounding ion plume. As a result, a larger electron extraction current can be obtained at the same collector bias voltage, and the current-jump transition can occur at a smaller magnitude of negative collector bias voltage. These results

suggest that the 60° and 90° configurations may position the RPN emission aperture within regions of ion plume that are more favorable for electron extraction.

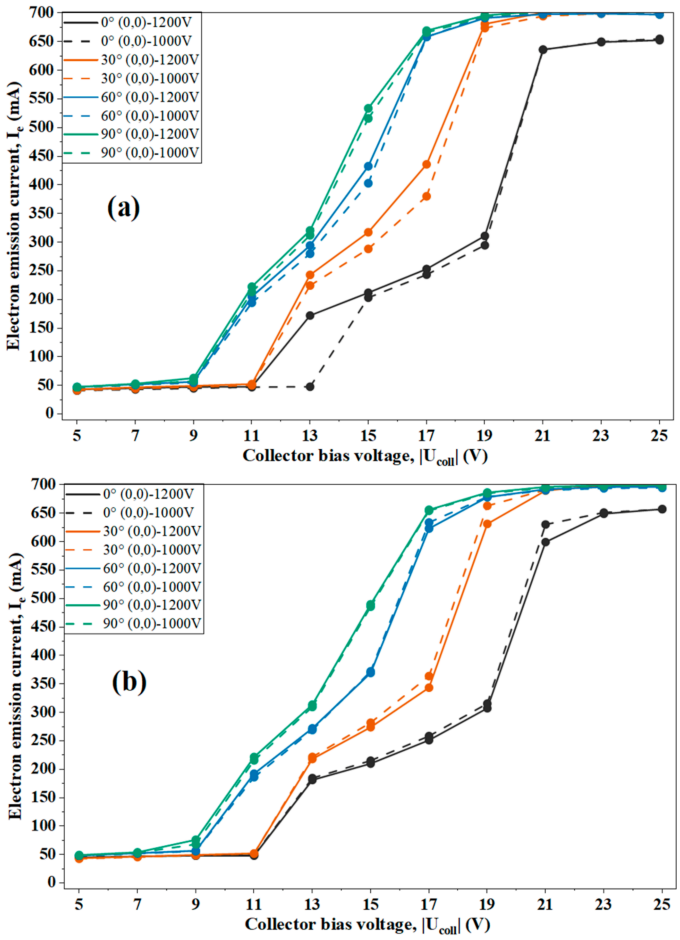



**Figure 9.** Variation in electron extraction current with collector bias voltage under different ion beam current conditions at the spatial position (0, 20). (**a**) RIT ion beam current: 310 mA; (**b**) RIT ion beam current: 440 mA.

To further investigate the spatial coupling between the RPN and the ion plume, the 90° configuration was selected as a representative case. The RIT ion beam current was maintained at 440 mA; the screen-grid voltage was set to 1200 V; and the collector bias voltage was set to −5 V, −11 V, and −17 V, respectively. The RPN position was varied along the X- and Y-axes using the positioning stage. The spatial distribution of the investigated positions is shown in Figure 10, and the corresponding electron extraction characteristics at different spatial coordinates are presented in Figure 11.

As shown in Figure 11, the electron extraction current of the RPN exhibits a clear dependence on spatial position. At Y = 40 mm, the electron extraction current generally increases as X moves from 20 mm toward −10 mm, and this trend is particularly evident under the 90° configuration. Meanwhile, the electron extraction current in the Y = 20–40 mm region is generally higher than that at Y = 0 mm, indicating the presence of a favorable spatial region within the investigated range. This spatial dependence may be associated with the transverse expansion of the ion plume during axial propagation and the resulting electron–ion spatial coupling. At Y = 0 mm, the RPN emission aperture is aligned with the RIT exit plane. At this position, the ion beam has just been extracted through the ion optics system and retains a relatively high degree of axial directivity. As the RPN is moved downstream to Y = 20–40 mm, the ion plume gradually expands in the transverse direction,

increasing the spatial overlap between the RPN emission aperture and the ion plume. This increased overlap may facilitate the transport of extracted electrons into the ion beam region and enhance local electron–ion charge compensation, thereby providing a more favorable electron transport path. At the same time, changes in the RPN position also modify the local plume potential and sheath conditions around the emission aperture. The combined effects of spatial overlap and local potential distribution may account for the enhanced electron extraction observed in the Y = 20–40 mm region compared with the Y = 0 mm position. When the magnitude of the collector bias voltage is increased to −17 V, relatively high electron extraction currents are obtained near X = −10 mm and Y = 20–40 mm. Under the 90° configuration, the electron extraction current reaches approximately 679.3 mA at (−10, 20) mm and approximately 673.0 mA at (−10, 40) mm. Considering the observed run-to-run variation of approximately 5 mA, these two positions are regarded as exhibiting comparable electron extraction currents rather than a clearly resolvable difference in extraction performance. Therefore, the region of X = −10 mm and Y = 20–40 mm is considered a favorable electron extraction region within the investigated range.

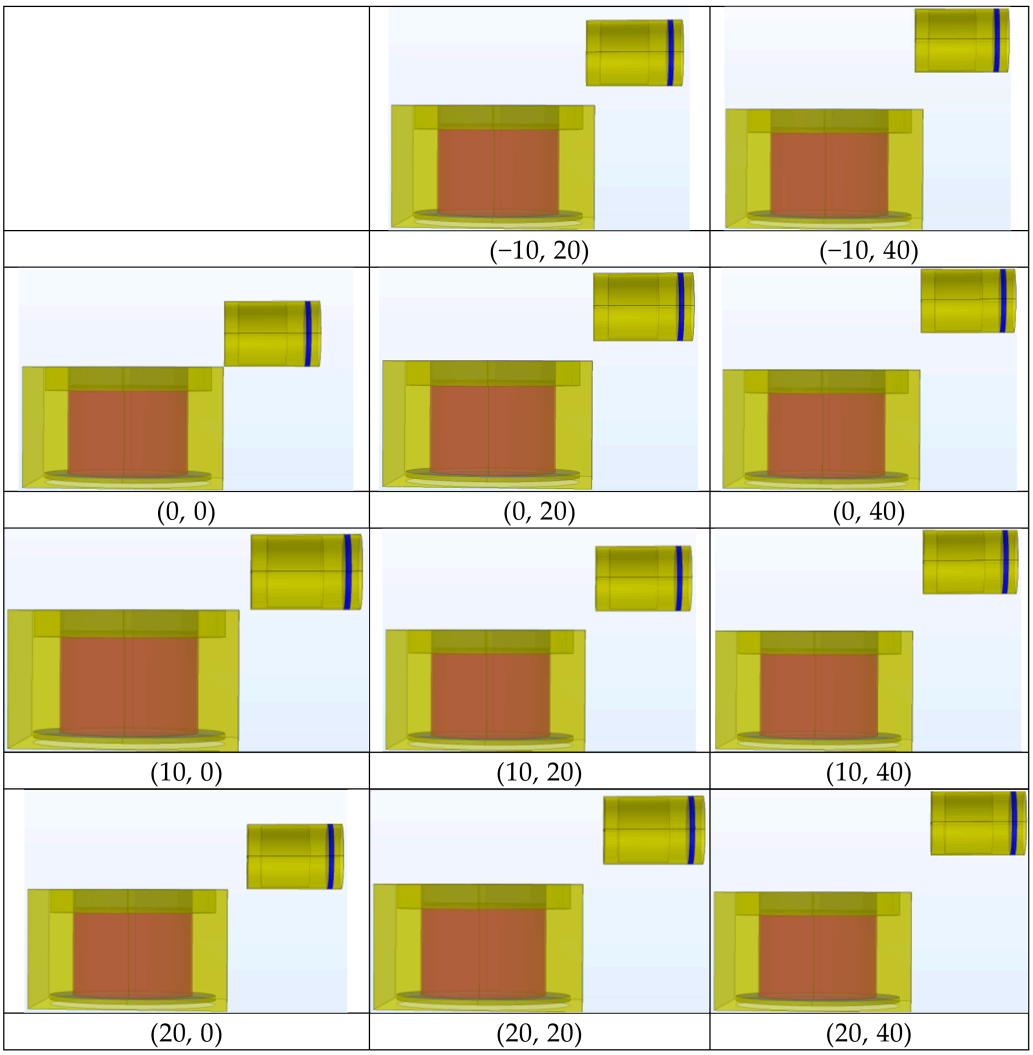



**Figure 10.** Schematic of the RPN arrangement under the 90° configuration.

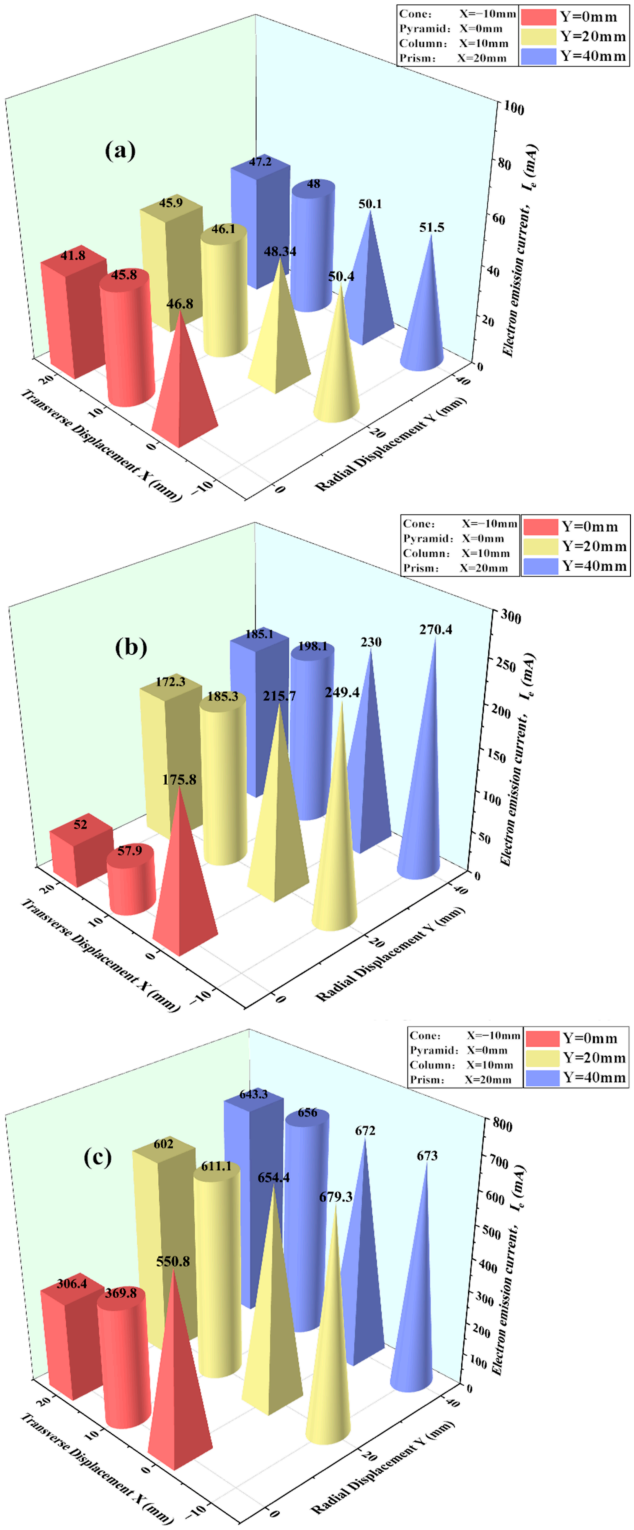



**Figure 11.** Spatial distribution of the electron extraction current at an ion beam current of 440 mA, a screen-grid voltage of 1200 V, and an installation angle of 90°. (**a**) Collector bias voltage: −5 V; (**b**) collector bias voltage: −11 V; (**c**) collector bias voltage: −17 V.

### *3.4. Spatial Matching Characteristics Between the RIT and RPN Based on the Equivalent Floating Potential*

To further evaluate the matching characteristics between the RIT and RPN at different spatial positions, experiments were conducted at an ion beam current of approximately 440 mA and a screen-grid voltage of 1200 V for the 60° and 90° configurations. For each

spatial position, the collector bias voltage was varied while the RPN electron extraction current was monitored. When the RPN electron extraction current became equal to the prescribed RIT ion beam current, the corresponding collector bias voltage was defined as the equivalent floating potential, $U_{eq}$. Thus, $U_{eq}$ was determined directly from the experimentally established current-matching condition. In this section, $U_{eq}$ is used as a comparative indicator of the current-matching behavior among the investigated spatial configurations. For the same ion beam current, a smaller magnitude of $U_{eq}$ indicates that current matching is achieved at a smaller magnitude of externally applied collector bias under the present ground-test conditions. Under practical on-orbit operation, when the electron extraction current of the RPN balances the ion beam current, a smaller magnitude of the floating potential indicates stronger coupling between the RPN and the ion plume. Therefore, the magnitude of the equivalent floating potential, $|U_{eq}|$, is used in this section as one of the parameters for evaluating the matching performance between the RIT and RPN. For the same ion beam current, if the RPN can provide an electron current equal to the ion beam current at a smaller magnitude of negative collector bias voltage, it indicates more favorable coupling conditions between electron extraction and the ion plume.

As shown in Figure 12, the experimental results show that the equivalent floating potential exhibits a clear dependence on spatial position under both installation angles. Overall, as the RPN is moved in the negative X-axis, the magnitude of the collector bias voltage required to achieve an electron extraction current of 440 mA gradually decreases. In particular, the region of X = −10 mm and Y = 20–40 mm exhibits relatively low equivalent floating potentials. Under the 60° configuration, $|U_{eq}|$ near (−10, 20) is approximately 14.7 V, representing one of the lower values for this installation angle. Under the 90° configuration, $|U_{eq}|$ near (−10, 40) is further reduced to approximately 13.5–14 V, which is the lowest value among all tested positions. Combined with the electron extraction current distributions obtained under fixed collector bias conditions, the results indicate that the region of X = −10 mm and Y = 20–40 mm not only exhibits a relatively high electron extraction capability at the same bias voltage but also requires a smaller collector bias-voltage magnitude to achieve the same electron current. This further indicates that this region provides more favorable coupling characteristics between the RIT and RPN. Among all tested configurations, the 90° configuration at (−10, 40) can be regarded as the preferred installation position within the present experimental range.

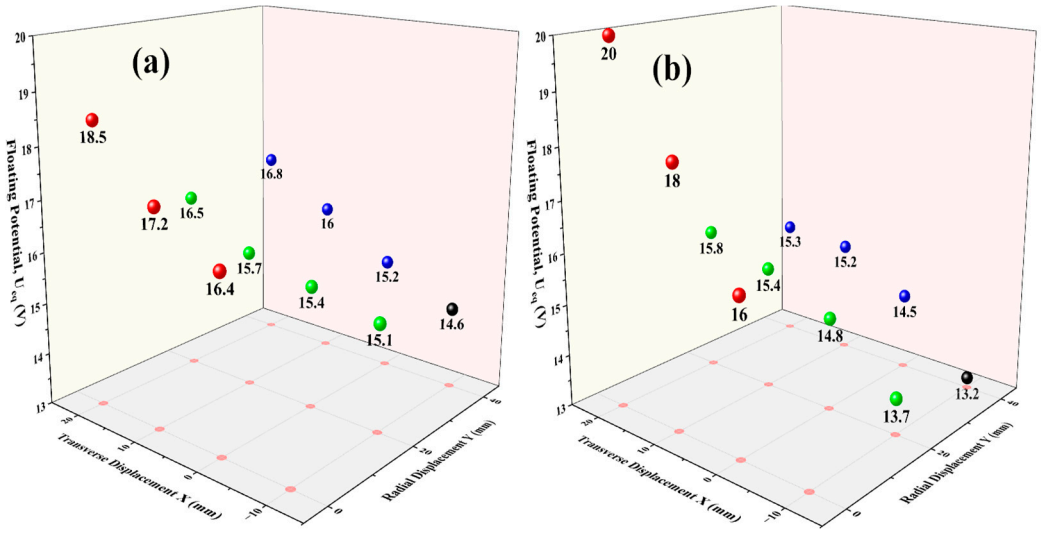



**Figure 12.** Spatial distribution of the equivalent floating potential at current-matching conditions under the (**a**) 60° and (**b**) 90° configurations.

## 4. Conclusions

In this study, an integrated RIT–RPN experimental system comprising an RIT-13 and an RPN-2.5 was established to investigate the effects of ion beam current, collector bias voltage, screen-grid voltage, and RPN spatial configuration on electron extraction characteristics in an actual ion-plume environment. Based on the steady-state current-balance criterion, the collector bias voltage at which the RPN electron extraction current becomes equal to the RIT ion beam current was defined as a current-balance-derived equivalent floating potential and used as a comparative parameter for evaluating the investigated RIT–RPN configurations. The main conclusions are as follows:

(1) The collector bias voltage is the primary parameter governing the electron extraction state of the RPN. As the magnitude of the negative bias voltage increases, the electron extraction current exhibits two distinct jumps, corresponding to transitions between different electron extraction states. The ion beam current mainly modulates the electron extraction state within the current-jump transition region, whereas the hysteresis between the increasing and decreasing bias-voltage sweeps remains weak under the investigated conditions.

(2) The RPN installation angle significantly affects the electron extraction characteristics. Compared with the 0° and 30° configurations, the 60° and 90° configurations reach the high-current electron extraction state at smaller magnitudes of negative collector bias voltage. Among the investigated configurations, the 90° configuration exhibits the most favorable overall electron extraction characteristics.

(3) The influence of screen-grid voltage on RPN electron extraction depends on the ion beam current and the electron-extraction state. At an ion beam current of approximately 310 mA, the 1200 V condition generally produces higher electron extraction current within the current-jump transition region, whereas an opposite trend is observed at approximately 440 mA under the 60° configuration, where the 1000 V condition reaches the high-current extraction state at a smaller magnitude of collector bias. Once the RPN enters the high-current electron extraction plateau, the difference between the 1000 V and 1200 V conditions decreases substantially.

(4) The electron extraction characteristics and equivalent floating potential exhibit a pronounced dependence on RPN spatial position. Within the investigated spatial range, the region near X = −10 mm and Y = 20–40 mm provides favorable conditions for electron extraction. In particular, the 90° configuration at (−10, 40) exhibits the smallest magnitude of the equivalent floating potential among the investigated positions and is therefore identified as the most favorable configuration among the tested positions for spatial matching between the RIT and RPN.

Future work will focus on RIT–RPN coupled operation under an electrical configuration that more closely represents the on-orbit floating condition. The externally applied collector-bias supply will be removed, and the RPN collector will be connected directly to the floating potential of the coupled system. Under this configuration, electron extraction from the RPN will no longer be actively controlled by an externally imposed bias voltage but will instead adjust self-consistently through the current balance between the RIT ion beam and the RPN electron emission. As the RIT ion beam current varies, the system floating potential is expected to respond to the resulting net charging condition and consequently modify the electron extraction condition of the RPN. Local plasma and ion-plume diagnostics will also be introduced using a Langmuir probe, a Faraday cup, and an E × B probe to characterize the plasma parameters near the RPN, the ion-current-density and beam spatial distributions, and the ion-species and associated velocity characteristics, respectively. By correlating these local plume properties with the RPN electron extraction characteristics and system floating potential, the coupling among the ion-plume distribution, local plasma

state, and electron extraction can be investigated quantitatively, providing further validation of the physical interpretations and current-matching relationships proposed in the present ground-based study.

**Author Contributions:** Conceptualization, J.Y. and L.M.; methodology, L.M.; software, L.M.; validation, H.H., L.D., Q.K., and J.H.; formal analysis, J.Y.; investigation, J.H.; resources, L.M.; data curation, J.Y.; writing—original draft preparation, J.Y.; writing—review and editing, J.G., L.M., and J.H.; visualization, J.Y.; supervision, J.H., J.G., L.D., Q.K., and H.H.; project administration, L.M.; funding acquisition, J.H. All authors have read and agreed to the published version of the manuscript.

**Funding:** This work was supported by the Strategic Priority Research Program of the Chinese Academy of Sciences, Grant No. XDA0470202, and Beijing Natural Science Foundation (L2602066).

**Data Availability Statement:** The dataset is available from the authors upon request.

**Conflicts of Interest:** The authors declare no conflicts of interest.

## References

1. McGrath, C.; Lowe, C.; Macdonald, M.; Hancock, S. Investigation of very low Earth orbits (VLEOs) for global spaceborne lidar. *CEAS Space J.* **2022**, *14*, 625–636. [CrossRef]
2. Crisp, N.H.; Roberts, P.C.E.; Livadiotti, S.; Oiko, V.; Edmondson, S.; Haigh, S.; Huyton, C.; Sinpetru, L.; Smith, K.; Worrall, S.; et al. The benefits of very low Earth orbit for Earth observation missions. *Prog. Aerosp. Sci.* **2020**, *117*, 100619. [CrossRef]
3. Yuxian, Y.; Jinyue, G.; Guanhua, F.; Hongwei, L.; Xian, M.; Jianwu, H.; Jinwen, C.; Wenhao, L.; Heji, H. Analysis of very-low Earth orbit flight system based on air-breathing electric propulsion technology. *Chin. J. Theor. Appl. Mech.* **2023**, *55*, 2835–2843. (In Chinese)
4. Wu, J.; Zheng, P.; Zhang, Y.; Tang, H. Recent development of intake devices for atmosphere-breathing electric propulsion. *Prog. Aerosp. Sci.* **2022**, *133*, 100848. [CrossRef]
5. Sun, A.B.; Feng, C.X.; Zhang, S.Y.; Zhang, G.J.; Jia, X.D.; Cui, Y.F.; Pu, Y.X.; Wu, C.C.; Geng, H.; Li, D.T. Research progress and prospects of VLEO air-breathing electric propulsion. *Spacecr. Environ. Eng.* **2025**, *42*, 239–255. (In Chinese)
6. Andreussi, T.; Ferrato, E.; Giannetti, V. A review of air-breathing electric propulsion: From mission studies to technology verification. *J. Electr. Propuls.* **2022**, *1*, 31. [CrossRef]
7. Löb, H.W. Ein elektrostatisches Raketentriebwerk mit Hochfrequenzionenquelle. *Astronaut. Acta* **1962**, *8*, 49–53.
8. Li, Y.H.; Chen, Y.C.; Liu, S.W.; Aslan, A.R. Prediction and optimization of thrust performance from plasma diagnostics in the inductively coupled plasma of an RF ion thruster. *Acta Astronaut.* **2023**, *208*, 130–141. [CrossRef]
9. Kuninaka, H.; Molina-Morales, P. Spacecraft charging due to lack of neutralization on ion thrusters. *Acta Astronaut.* **2004**, *55*, 27–38. [CrossRef]
10. Nishii, K.; A Levin, D. Kinetic simulation of ion thruster plume neutralization in a vacuum chamber. *Plasma Sources Sci. Technol.* **2023**, *32*, 11. [CrossRef]
11. Saridede, E.; Celik, M. $LaB_6$ hollow cathode with a novel graphite heater. *Vacuum* **2023**, *216*, 112383. [CrossRef]
12. Polk, J.E.; Capece, A.M. Materials characterization of impregnated W and W–Ir cathodes after oxygen poisoning. *Appl. Surf. Sci.* **2015**, *338*, 27–34. [CrossRef]
13. Weis, S.; Schartner, K.H.; Löb, H.; Feili, D. Development of a capacitively coupled insert-free RF-neutralizer. In Proceedings of the 29th International Electric Propulsion Conference, Princeton, NJ, USA, 31 October–4 November 2005.
14. Godyak, V.A.; Raitses, Y.; Fisch, N.J. RF plasma cathode-neutralizer for space applications. In Proceedings of the 30th International Electric Propulsion Conference, Florence, Italy, 17–20 September 2007.
15. Raitses, Y.; Hendryx, J.K.; Fisch, N.J. A parametric study of electron extraction from a low frequency inductively coupled RF-plasma source. In Proceedings of the 31st International Electric Propulsion Conference, Ann Arbor, MI, USA, 20–24 September 2009.
16. Hatakeyama, T.; Irie, M.; Watanabe, H.; Okutsu, A.; Aoyagi, J.; Takegahara, H. Preliminary Study on Radio Frequency Neutralizer for Ion Engine. In Proceedings of the 30th International Electric Propulsion Conference, Florence, Italy, 17–20 September 2007.
17. Watanabe, H.; Okuma, T.; Aoyagi, J.; Takegahara, H. Research and Development on Inductively Coupled Plasma Cathode for Ion Engines. In Proceedings of the 31st International Electric Propulsion Conference, Ann Arbor, MI, USA, 20–24 September 2009.
18. Longmier, B.W.; Hershkowitz, N. "Electrodeless" Plasma Cathode for Neutralization of Ion Thrusters. In Proceedings of the 41st AIAA/ASME/SAE/ASEE Joint Propulsion Conference & Exhibit, Tucson, AZ, USA, 10–13 July 2005.
19. Longmier, B.; Hershkowitz, N. Development Status of the Nonambipolar Electron Source. In Proceedings of the 30th International Electric Propulsion Conference, Florence, Italy, 17–20 September 2007.

20. Baalrud, S.D.; Longmier, B.; Hershkowitz, N. Equilibrium states of anodic double layers. *Plasma Sources Sci. Technol.* **2009**, *18*, 035002. [CrossRef]
21. Jahanbakhsh, S.; Satir, M.; Celik, M. Study of electron current extraction from a radio frequency plasma cathode designed as a neutralizer for ion source applications. *Rev. Sci. Instrum.* **2016**, *87*, 02B922. [CrossRef] [PubMed]
22. Jianwu, H.; Longfei, M.; Senwen, X.; Chu, Z.; Li, D.; Qi, K. Study of electron-extraction characteristics of an inductively coupled radio-frequency plasma neutralizer. *Plasma Sci. Technol.* **2018**, *20*, 025403. [CrossRef]
23. Li, X.D.; Zhang, X.M.; Li, J.P.; Zhang, T.P.; Sun, X.F. Numerical simulation and experimental study of radio frequency electron source. *J. Propuls. Technol.* **2019**, *40*, 2394–2400. (In Chinese)
24. Xu, Z.; Wang, P.; Hua, Z.; Cong, S.; Yu, S. Numerical simulation and experimental research on an inductively coupled RF plasma cathode. *Plasma Sci. Technol.* **2022**, *24*, 015404. [CrossRef]
25. Fu, J.H.; Ma, L.F.; He, J.W.; Luo, J.; Kang, Q.; Duan, L. Electron extraction characteristics of a 1A-level RF inductively coupled plasma neutralizer. *J. Propuls. Technol.* **2024**, *45*, 2306074. (In Chinese)
26. Zorn, J.; Bräumer, K.J.; Rodriguez, R.S.; Wölki, A.R.; Keil, K.; Komjagin, A.; Bremer, F.B.; Hellbert, A.; Reuß-Hennschen, M.; Kaufmann, A.; et al. Characterization of the performance of a RIT-10 and rf-neutralizer for an ABEP system. *J. Electr. Propuls.* **2025**, *4*, 68. [CrossRef]
27. Neumann, H.; Scholze, F.; Tartz, M.; Leiter, H. A cathodeless RF plasma bridge neutralizer and results of the first coupled test with the RIT 22 ion thruster. In Proceedings of the 2nd Space Propulsion Conference, San Sebastian, Spain, 3–6 May 2010.
28. Scholze, F.; Tartz, M.; Neumann, H. Inductive coupled radio frequency plasma bridge neutralizer. *Rev. Sci. Instrum.* **2008**, *79*, 02B724. [CrossRef] [PubMed]
29. Sommerville, J.D.; King, L.B. Hall-effect thruster–cathode coupling, Part I: Efficiency improvements from an extended outer pole. *J. Propuls. Power* **2011**, *27*, 744–753. [CrossRef]
30. Sommerville, J.D.; King, L.B. Hall-effect thruster–cathode coupling, Part II: Ion beam and near-field plume. *J. Propuls. Power* **2011**, *27*, 754–767. [CrossRef]


**Disclaimer/Publisher's Note:** The statements, opinions and data contained in all publications are solely those of the individual author(s) and contributor(s) and not of MDPI and/or the editor(s). MDPI and/or the editor(s) disclaim responsibility for any injury to people or property resulting from any ideas, methods, instructions or products referred to in the content.